ARTICLE

Bimetallic Compound Catalysts With Multiple Active Centers for Accelerated Polysulfide Conversion in Li-S Batteries

Wu-Xing Hua [a,#], Jing-Yi Xia [a,#], Zhong-Hao Hu [a], Huan Li [a], Wei Lv [b,*], Quan-Hong Yang [a,*]

[a] Tianjin Key Laboratory of Advanced Carbon and Electrochemical Energy Storage, School of Chemical Engineering and Technology, Tianjin University, Tianjin, 300072, China
[b] Shenzhen Key Laboratory for Graphene-based Materials and Engineering Laboratory for Functionalized Carbon Material, Tsinghua Shenzhen International Graduate School, Tsinghua University, Shenzhen, 518055, China

Abstract

Practical applications of lithium-sulfur (Li-S) batteries are hindered mainly by the low sulfur utilization and severe capacity fading derived from the polysulfide shuttling. Catalysis is an effective remedy to those problems by promoting the conversion of polysulfides to reduce their accumulation in the electrolyte, which needs the catalyst to have efficient adsorption ability to soluble polysulfides and high activity for their conversion. In this work, we have proposed a bimetallic compound of $NiCo_2S_4$ anchored onto sulfur-doped graphene (NCS@SG) to fabricate a catalytic interlayer for Li-S batteries. Compared to CoS, the $NiCo_2S_4$ demonstrated much higher catalytic activity toward sulfur reduction reaction due to its multiple anchoring and catalytic active sites derived from the coordination of the bimetallic centers. As a result, the NCS@SG interlayer dramatically improved the specific capacity, rate performance, and cycling stability of Li-S batteries. Especially, when the areal sulfur loading of the NCS@SG battery increased to 15.3 $mg \cdot cm^{-2}$, the high-capacity retention of 93.9% could be achieved over 50 cycles.

Keywords: Lithium-sulfur batteries; Lithium polysulfides; Catalysis; Bimetallic sulfide catalyst; Shuttle effect

1. Introduction

Lithium-sulfur (Li-S) batteries show great promise as the next-generation energy storage devices [1−3]. However, they suffer from pronounced capacity fading during cycling. One of the major causes is the shuttling of lithium polysulfide intermediates (LiPSs, Li_2S_n, $3 \leq n \leq 8$), predominantly resulting in continuous loss of active material and poor coulombic efficiency [4,5]. The conventional solution is to physically confine or chemically trap the LiPSs in the cathode side [6−8], but they are passive solutions to prevent the dissolution of LiPSs into the electrolyte [9,10]. Consequently, the dissolved LiPSs tend to be transported from the cathode side to the anode side driven by the concentration gradient, which becomes much more serious with high sulfur loadings [11]. Recently, catalysis has been proposed to accelerate the conversion of the soluble LiPSs to solid products, decreasing their accumulation in the electrolyte [12−16]. Various catalysts, such as metal oxides [17,18], sulfides [19,20], nitrides [21,22], phosphides [23,24] and their heterostructures [25−27] have been used in Li-S batteries. However, the single compound catalyst cannot balance the adsorption and desorption of LiPSs, resulting in poor catalytic activities.

Received 30 July 2022; Received in revised form 23 August 2022; Accepted 15 September 2022
Available online 19 September 2022

* Corresponding author, Wei Lv, Tel: (86-755)86964142, E-mail address: lv.wei@sz.tsinghua.edu.cn.
* Corresponding author, Quan-Hong Yang, Tel: (86-22)27401097, E-mail address: qhyangcn@tju.edu.cn.
[#]Wu-Xing Hua and Jing-Yi Xia contributed equally to this work.

https://doi.org/10.13208/j.electrochem.2217006

Therefore, the catalysts with multiple anchoring and catalytic active centers are highly required to provide proper adsorption ability to LiPSs and accelerate their conversion.

The catalytic sites for sulfur redox reaction can be realized through the construction of subsurface defects and vacancies or cooperation of two different metal components. Recently, Zhao et al. [28] obtained a highly active cubic Ni_3FeN with abundant vacant defects around the nickel site for polysulfide catalysis by introducing an extrinsic metal (iron) in Ni_3N, exhibiting superb rate performance. Zeng et al. [29] designed a Fe-Co bimetallic alloy catalyst, which enhanced the entrapping-conversion processes of polysulfides. It is known that the atomic radius of Ni atom is close to that of Co atom and their outer shell electronic structures are similar (Ni: $3d^84s^2$; Co $3d^74s^2$), which would help to form the bimetallic Ni-Co, avoiding phase separation issues [29]. Besides, metal sulfides are widely used in Li-S batteries due to their easy preparation, good electrical conductivity, and high catalytic performance [30,31], suggesting a direction to design a high performance bimetallic sulfide catalyst.

Herein, we demonstrate that combining the Ni and Co to produce a highly active $NiCo_2S_4$ catalyst can effectively promote polysulfide conversion. The synthesized $NiCo_2S_4$ catalyst loaded onto the sulfur-doped graphene (NCS@SG) is used as a catalytic interlayer, where the sulfur-doped graphene functions as a physical barrier to block polysulfide shuttling at the same time. Thus, the assembled battery showed remarkable capacity retention at a high sulfur loading of 15.3 $mg \cdot cm^{-2}$ as the diffusion and shuttling of LiPSs were effectively suppressed. This work enlightens the great potential of bimetallic compound catalysts for high-performance Li-S batteries.

2. Experimental

2.1. Preparations of NCS@SG, CS@SG and SG composites

The graphene oxide (GO) was synthesized by the modified Hummers' method as reported previously [32]. The NCS@SG was synthesized via a facile one-pot solvothermal method and the following heat treatment. In typical, the dispersion of GO (2 $mg \cdot mL^{-1}$) was obtained by an ultrasonication treatment of graphite oxide (160 mg) in ethylene glycol (80 mL) for 2 h. Then, 0.2 mmol $Ni(AC)_2$ and 0.4 mmol $Co(AC)_2$ were added to the above dispersion with heating and stirring at 80 °C for 1 h. Afterward, 1.2 mmol thiourea was added to the above solution. The mixture was transferred to a 100 mL Telfon-lined autoclave and heated at 200 °C for 6 h. The obtained sample was rinsed with deionized water several times and freeze-dried for 48 h. Finally, the product was heated at 500 °C for 1 h with a heating rate of 5 $°C \cdot min^{-1}$ in an Ar atmosphere. For comparison, CoS catalyst loaded onto the sulfur-doped graphene (CS@SG) without adding $Co(AC)_2$, and sulfur-doped graphene (SG) without adding $Ni(AC)_2$ and $Co(AC)_2$ were synthesized with the same procedure.

2.2. Preparations of CNT/S cathode with NCS@SG, CS@SG or SG interlayer

The carbon nanotube/sulfur (CNT/S) composite was prepared by a simple melt-diffusion method [33]. Typically, a mixture of CNT and sulfur with a mass ratio of 3:7 was ground uniformly and heated at 155 °C for 12 h. The CNT/S cathode was prepared by mixing CNT/S powder, conductive agent (CNT) and poly(vinylidene fluoride) as a binder with the ratio of 8:1:1 dissolved in N-methyl-2-pyrrolidone (NMP) to form a slurry, which was then coated onto a carbon-coated aluminum foil current collector and vacuum-dried at 55 °C overnight. The total sulfur content in the cathode was 56%. The NCS@SG, CS@SG or SG interlayer was coated on the CNT/S cathode as previously reported [34]. Typically, the NCS@SG, CS@SG or SG composite was dispersed in NMP to form a slurry that was then coated on the dried CNT/S cathodes by a spreader. After drying, Al foil to cover both the cathode and interlayer was cut into circles of a diameter of 10 mm. The mass of the NCS@SG, CS@SG or SG interlayer was ca. 0.2 $mg \cdot cm^{-2}$ and the sulfur loading of each electrode was ca. 1.0 $mg \cdot cm^{-2}$.

2.3. Preparation of a freestanding high sulfur-loaded cathode with NCS@SG interlayer

The freestanding high sulfur-loaded cathode was prepared as reported previously [20]. In typical, CNT/S composite, conductive agent (CNT), and polytetrafluoroethylene (PTFE) binder with a mass ratio of 80:15:5 were dissolved in ethanol under ultrasonication, which was evaporated at room temperature to form a slurry. Afterward, the prepared slurry was rolled into a thin sheet, which was cut into circular electrodes as freestanding CNT/S cathodes with a diameter of 10 mm. The diameter shrank to ca. 8.0 mm after vacuum drying at 55 °C overnight. To introduce the NCS@SG interlayer, the prepared NCS@SG composite was added to ethanol and ultrasonically dispersed to

form a homogeneous solution, which was then vacuum filtrated on the separator to obtain the modified separator. Photos of the as-prepared NCS@SG interlayers are shown in Fig. S1.

2.4. Assembly of the symmetric batteries

Li_2S_6 electrolyte was prepared via adding Li_2S and sulfur powder with a molar ratio of 1:5 to 1.0 mol·L^{-1} LiTFSI in a DOL/DME solution (1:1, *V*/*V*). The concentration of the obtained Li_2S_6 electrolyte was 0.2 mol·L^{-1}. The commercial carbon paper (CP) was punched into small disks with a diameter of 10.0 mm. The prepared NCS@SG or CS@SG composite was loaded onto CP disks and is named as CP-NCS@SG or CP-CS@SG electrode. The loading methods were the same as those previously reported [20]. Two identical electrodes were assembled into a standard 2032 coin battery with Celgard 2400 as the separator and 40 μL of Li_2S_6 electrolyte (20 μL for each side of the separator).

2.5. Measurement for the nucleation of Li_2S

Li_2S_8 electrolyte was prepared by adding Li_2S and sulfur powder with a molar ratio of 1:7 to tetraglyme and stirred at 60 °C for 24 h. The concentration of the Li_2S_8 electrolyte was 0.2 mol·L^{-1}. NCS@SG or CS@SG powder was loaded onto CP with a diameter of 10 mm (denoted CP-NCS@SG or CP-CS@SG) for use as the cathode and lithium foil was used as the anode. 20 μL Li_2S_8 electrolyte was used as the catholyte and 20 μL of the electrolyte without Li_2S_8 was used as the anolyte. The assembled batteries were first galvanostatically discharged under a current of 0.112 mA until the voltage decreased to 2.06 V and then discharged potentiostatically at 2.05 V for Li_2S nucleation and growth [14].

2.6. Battery assembly and electrochemical measurements

The battery with NCS@SG, CS@SG or SG interlayer (denoted as NCS@SG, CS@SG or SG battery) was assembled in an Ar-filled glovebox using lithium foil as the anode, Celgard 2400 as the separator and 1.0 mol·L^{-1} LiTFSI in a DOL/DME solution (1:1, *V*/*V*) with 1.0 wt% $LiNO_3$ as the electrolyte. The E/S ratios were about 20 and 15 μL·mg^{-1} for the normal Li-S batteries and freestanding high sulfur-loading batteries, respectively. The galvanostatic discharge/charge measurements were conducted through Neware battery test system with a potential range of 1.7−2.7 V (*vs.* Li^+/Li). Cyclic voltammetric (CV) results of the symmetric batteries were obtained using an Autolab workstation at a scan rate of 20 mV·s^{-1} with a voltage window between −0.8 V and 0.8 V, and EIS measurements were carried out with a frequency range of 10^{-2}−10^5 Hz on the same workstation. The temperature-dependent CV measurements were conducted on an IVIUM workstation at a scan rate of 0.1 mV·s^{-1}.

2.7. Structure characterizations

The morphologies and structures of the samples in this work were examined by TEM (JEM−2100 F, Japan). The crystal structures of the samples were characterized by X-ray diffraction (Bruker D-8, Germany) with Cu *K* radiation (λ = 0.154 nm). Thermogravimetric (TG, Rigaku, Japan) analysis was performed in the air atmosphere from room temperature to 1000 °C at a heating rate of 10 °C per minute to calculate the content of sulfide in the composite. XPS data were recorded by an ESCALAB Xi^+ (Thermo Fisher Scientific) with Al *Kα* source to analyze the surface species and their chemical states.

3. Results and discussion

The NCS@SG was synthesized through a one-pot solvothermal and the following heat treatment process. During the solvothermal reaction, the $Co(AC)_2$, $Ni(AC)_2$, thiourea, and graphene oxide (GO) were used as precursors, and ethylene glycol as the solvent (Fig. 1a). Note that ethylene glycol acts as a mild reducing agent to reduce GO and a chelating agent to avoid agglomeration of nanoparticles at the same time. The thiourea was used as the sulfur source to form metal sulfides, and simultaneously, traces of sulfur were doped into the reduced graphene oxide (rGO) during the reaction. The final products were characterized by X-ray diffraction (XRD) (Fig. 1b), and the diffraction peaks at 26.8°, 31.6°, 38.3°, 50.5° and 55.3° well match the (220), (311), (400), (511) and (440) planes for the cubic phase of $NiCo_2S_4$ (PDF#20−0782) [35]. The XRD patterns in Fig. 1c also confirm the formation of a hexagonal phase CoS (PDF#65−3418). The incorporation of nickel induces the hexagonal-to-cubic phase transformation. The morphologies of the prepared NCS@SG and CS@SG were characterized by transmission electron microscopy (TEM) (Fig. 1d and e), showing the uniformly dispersed $NiCo_2S_4$ and CoS on the sulfur-doped graphene (SG) substrate, and both $NiCo_2S_4$ and CoS are found as nanoparticles of 15−35 nm in size. The EDX elemental maps (Fig. S2) illustrate

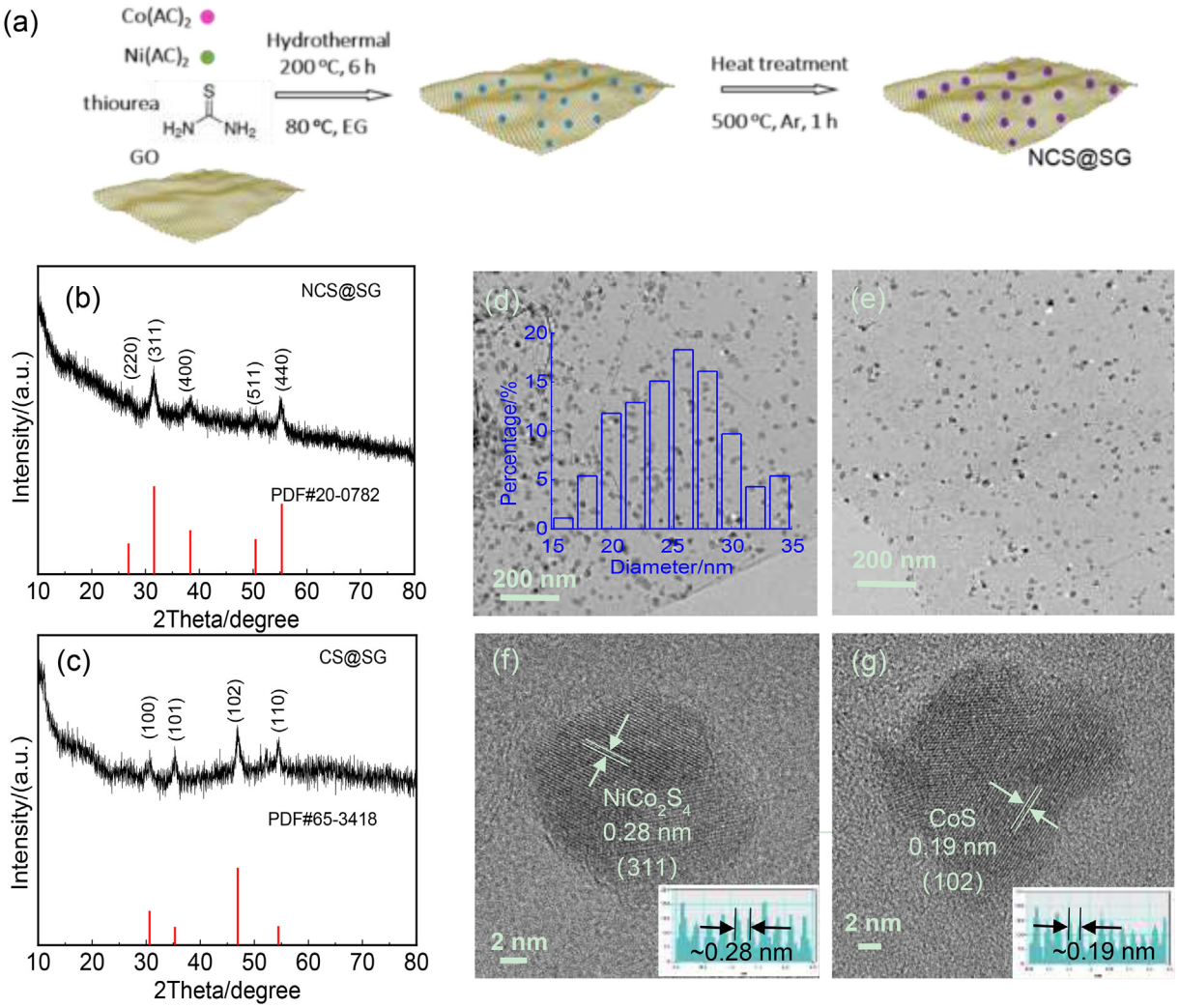

Fig. 1. (a) The fabrication process of the NCS@SG hybrid; XRD patterns of the prepared (b) NCS@SG and (c) CS@SG hybrids; TEM images of (d, f) NCS@SG and (e, g) CS@SG hybrids.

the homogenous distributions of Ni, Co, C and S elements in the NCS@SG, which ensures the uniform distribution of Li_2S deposition and dissolution during the battery cycling. The high-resolution TEM image in Fig. 1f clearly shows the lattice fringe of 0.28 nm spacing of (311) crystal plane of $NiCo_2S_4$, and the crystal of CS@SG in Fig. 1g illustrates a lattice fringe of 0.19 nm, corresponding to the (102) plane of CoS.

To determine the contents of $NiCo_2S_4$ and CoS in the NCS@SG and CS@SG hybrids, thermogravimetric analysis (TGA) was conducted under the air atmosphere at a heating rate of 10 °C·min^{-1} (Fig. 2a and b). Between 200 and 430 °C, the weight increase is ascribed to the oxidation of sulfides to sulfates, and the weight loss at 430−560 °C is associated with the decomposition of rGO. In order to identify the final products over 660 °C, the prepared NCS@SG and CS@SG hybirds were calcined at 850 °C in air for 1 h. The XRD patterns in Fig. 2c and d confirm that the calcined products of NCS@SG were NiO and Co_3O_4, and of CS@SG was Co_3O_4. Therefore, the contents of $NiCo_2S_4$ and CoS in the NCS@SG and CS@SG can be calculated to be 33.7 wt% and 34.1 wt%, respectively, accordingly, the contents of $NiCo_2S_4$ and CoS in the whole sulfur cathode are about 4.7 wt% and 4.8 wt%, respectively.

Effective adsorption of LiPSs is the precondition for their fast conversion on the catalyst. Therefore, X-ray photoelectron spectroscopy (XPS) was used to analyze the surface states of NCS@SG and CS@SG before and after the adsorbing polysulfide (Li_2S_6). As shown in Fig. 3a, the Co *2p* core-level XPS spectrum in the pristine CoS can be deconvoluted into six peaks, in which two pair peaks of 778.5, 793.6 eV and 781.1, 796.9 eV are corresponding to Co−S and Co−O bonds, respectively. The peak positions are not changed after the adsorption of Li_2S_6, indicating the poor interaction

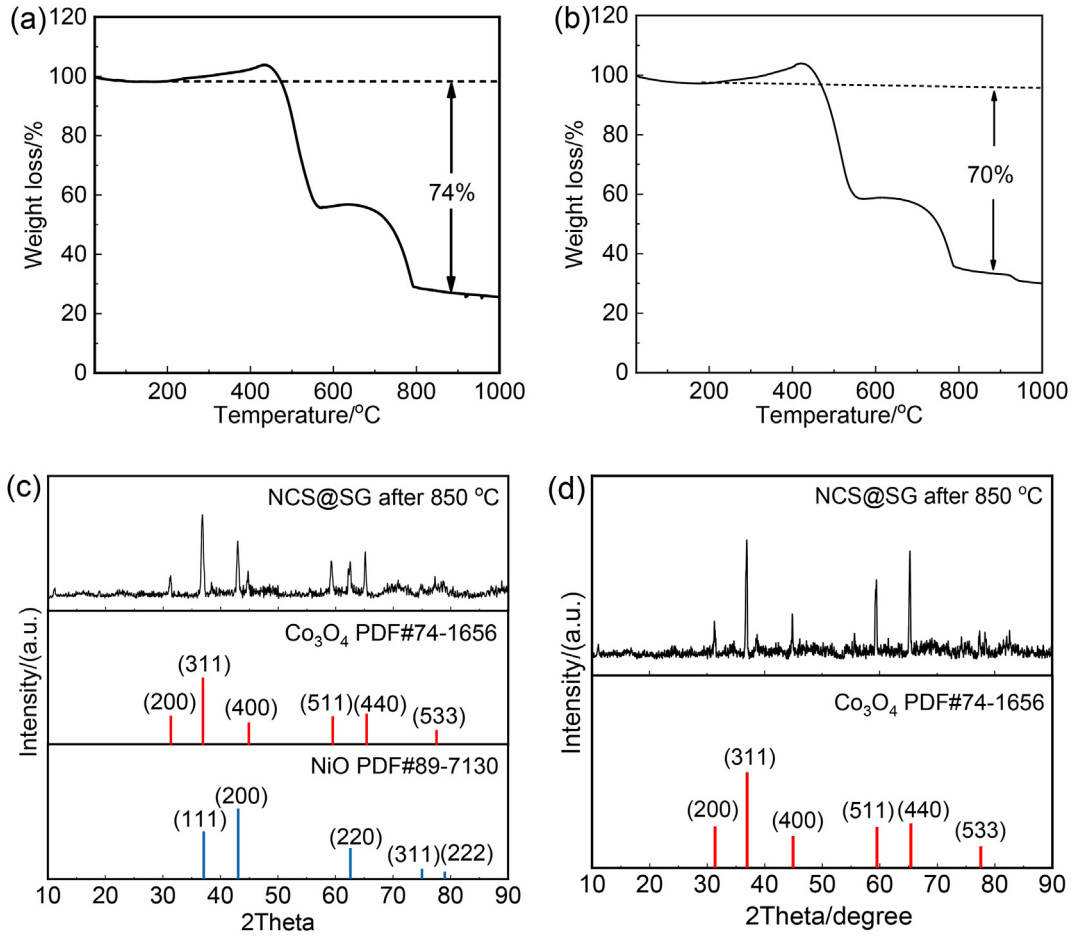

Fig. 2. TGA curves of (a) NCS@SG and (b) CS@SG hybrids; XRD patterns of (c) NCS@SG and (d) CS@SG after calcination at 850 °C for 1 h in air.

between CoS and polysulfides. However, for $NiCo_2S_4$, the characteristic peaks of Co *2p* and Ni *2p*, corresponding to the Co−S and Ni−S bonds, respectively, show obvious upshift to higher binding energy, indicating the transfer of electrons from $NiCo_2S_4$ to electron-rich S atoms in Li_2S_6 (Fig. 3b and c) [28,36,37]. These results confirm that the $NiCo_2S_4$ catalyst can provide multiple active centers to adsorb the soluble LiPSs. In addition, the effective interaction between $NiCo_2S_4$ and LiPSs can also be verified by the S *2p* spectra. As shown in Fig. 3d, the S *2p* peaks located at 161.3 and 162.4 eV in the pristine $NiCo_2S_4$ are attributed to the metal-sulfur (M−S) bond [38]. After the adsorption experiment, the peaks of the M−S bond shift to lower binding energies, demonstrating the strong interaction between $NiCo_2S_4$ and Li_2S_6.

CV curves of Li-S batteries with CNT/S coupled NCS@SG, CS@SG or SG interlayer as the cathode and lithium foil as the anode (named as NCS@SG, CS@SG or SG battery) are shown in Fig. 4a. During the discharge process, the two reduction peaks at ca. 2.3 V (C_1) and 2.0 V (C_2) are, respectively, attributed to the reductions of sulfur to Li_2S_n and then to the discharge products Li_2S_2/Li_2S. On the forward scan, two apparent oxidation peaks at ca. 2.3 V (A_1) and 2.4 V (A_2) are observed, corresponding to the conversions from Li_2S to Li_2S_n, and finally to elemental sulfur, respectively [17,39]. For the battery with NCS@SG, a remarkable positive shift in the reduction peaks and a negative shift in the oxidation peaks indicate the better catalytic activity of the $NiCo_2S_4$ catalyst [40,41]. Besides, the battery with NCS@SG shows higher current intensity, and narrower peak separation between the reduction peak (C_2) and oxidation peak (A_1) than those of the other two batteries, suggesting the enhanced conversions from LiPSs to Li_2S and then to LiPSs with the help of $NiCo_2S_4$ catalyst [40]. These results demonstrate that the accumulation of LiPSs in the electrolyte can be greatly alleviated with a $NiCo_2S_4$ catalyst.

Tafel plots are plotted to evaluate the catalytic activities of $NiCo_2S_4$ and CoS catalysts. As shown in Fig. 4b, the battery with NCS@SG shows a smaller Tafel slope of 48.3 $mV \cdot dec^{-1}$ than those

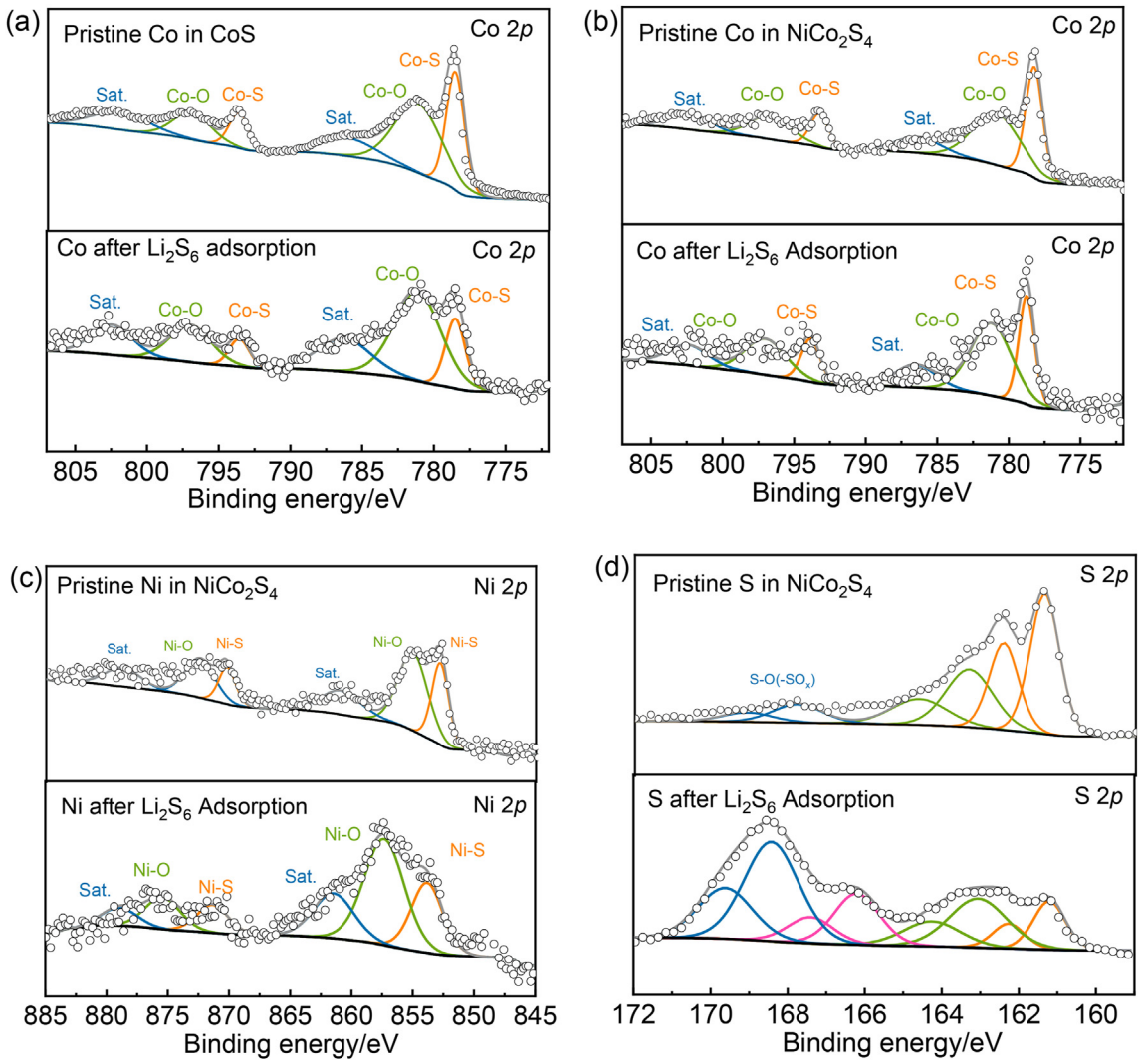

Fig. 3. (a) XPS spectra of Co 2p for CS@SG before and after Li_2S_6 adsorption. XPS spectra of (b) Co 2p, (c) Ni 2p and (d) S 2p for NCS@SG before and after Li_2S_6 electrolyte adsorption.

with CS@SG (95.7 $mV \cdot dec^{-1}$) and SG (188.6 $mV \cdot dec^{-1}$), indicating the fast conversion from Li_2S_n to Li_2S with $NiCo_2S_4$ catalyst [17,42]. The electrochemical impedance spectroscopic (EIS) curves of the Li-S batteries with NCS@SG, CS@SG and SG interlayers at open-circuit voltage are shown in Fig. 4c. The Nyquist plots consist of two parts: a semicircle at high frequency and a sloped line at low frequency, which, respectively, correspond to the charge transfer resistance (R_{ct}) and ion diffusion process. Based on the equivalent circuit fitting results, the battery with NCS@SG interlayer shows much smaller R_{ct} value (30.2 Ω) than the batteries with CS@SG interlayer (119.5 Ω) and SG interlayer (155.8 Ω), confirming that the $NiCo_2S_4$ effectively reduces the charge transfer resistance due to its good conductivity and catalytic activity [43]. The activation energy (E_a) is an important parameter to describe the catalytic activity of catalysts [20]. It is widely accepted that the conversion of Li_2S_4 to Li_2S_2/Li_2S is the rate-determining step [15]. To obtain the E_a in this step, the temperature-dependent CV measurements were conducted (Fig. 4d and e). The peak current (j) is proportional to the reaction rate (k), thus the E_a can be calculated according to the Arrhenius equation $j \propto k = A \times e^{-Ea/RT}$, where R is the gas constant, A is the pre-exponential factor, and T is the temperature [20,44]. The calculated results are shown in Fig. 4f, and the battery with NCS@SG shows a much lower E_a (12.1 $kJ \cdot mol^{-1}$) for the conversion from Li_2S_4 to Li_2S_2/Li_2S than that of the CS@SG battery (22.9 $kJ \cdot mol^{-1}$), confirming the high catalytic activity of $NiCo_2S_4$ catalyst. The dissolution of Li_2S is an important process, which affects the utilization of active sulfur [45]. The conversion of Li_2S to soluble Li_2S_n is accelerated with $NiCo_2S_4$ catalyst as the activation energy for

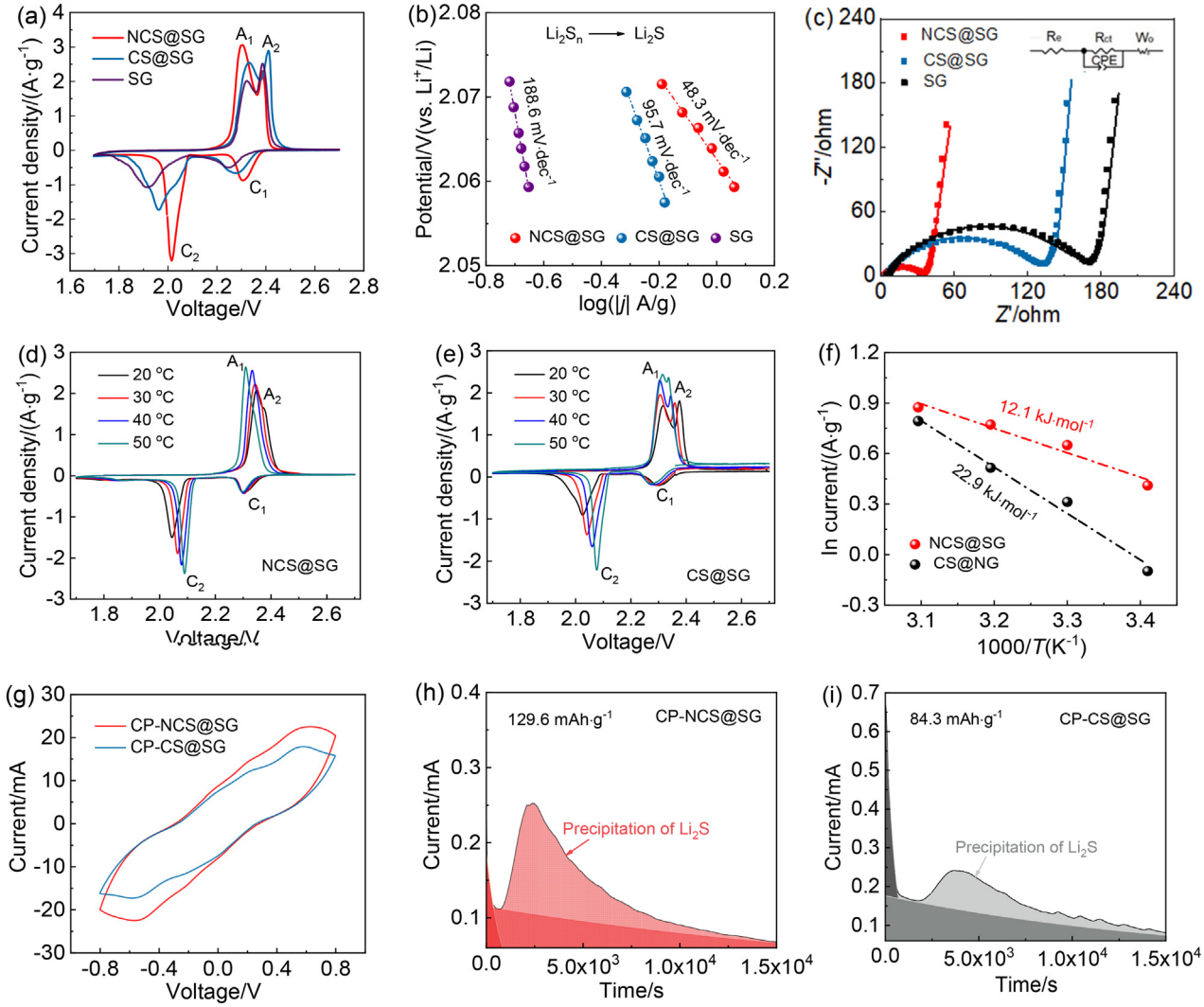

Fig. 4. (a) CV curves at 0.1 mV·s^{-1} for the batteries with NCS@SG, CS@SG and SG interlayers; (b) Tafel plots corresponding to the reductions of Li_2S_n to Li_2S; (c) EIS curves of Li-S batteries with NCS@SG, CS@SG and SG interlayers (the inset is the equivalent circuit); (d–e) CV curves for the batteries with NCS@SG (d) and CS@SG (e) interlayers at 20, 30, 40, and 50 °C; (f) Relationship between the peak current of the Li_2S_4 conversion step in the CV curves and temperature; (g) CV curves of symmetrical batteries with CP-NCS@SG and CP-CS@SG with Li_2S_6 in the electrolyte at 20 mV·s^{-1}; (h–i) Potentiostatic discharge curves of the Li_2S deposition tests using CP-NCS@SG (h) and CP-CS@SG (i) electrodes.

the oxidation of Li_2S to Li_2S_n is decreased by 2.9 kJ·mol^{-1} for the battery with NCS@SG interlayer compared to the battery with CS@SG interlayer in Fig. S3. This result indicates that the $NiCo_2S_4$ catalyst can catalyze the deposition and dissolution of Li_2S (Li_2S_n-to-Li_2S and Li_2S-to-Li_2S_n).

The liquid-liquid conversion kinetics of LiPSs was probed through CV measurement using the symmetric batteries with Li_2S_6 in the electrolyte (Fig. 4g). The battery with CP-NCS@SG exhibited a higher current density than that with CP-CS@SG at 20 mV·s^{-1}, indicating the enhanced conversion of LiPSs with the $NiCo_2S_4$ catalyst [38]. Potentiostatically Li_2S precipitation was tested to evaluate the conversion from LiPSs to Li_2S. The coin batteries for the tests were assembled with the NCS@SG or CS@SG loaded on carbon fiber paper (CP) as the cathode, coupled with Li anode and Li_2S_8 electrolyte. As shown in Fig. 4 h–i, the initial nucleation of Li_2S was earlier on CP-NCS@SG than that on CP-CS@SG. Moreover, the precipitation capacity of Li_2S on CP-NCS@SG (129.6 mAh·g^{-1}) was higher than that on CP-CS@SG (84.3 mAh·g^{-1}), confirming that the $NiCo_2S_4$ catalyst accelerates the LiPSs-to-Li_2S conversion, and then, reducing their accumulation in the electrolyte to suppress the shuttle effect [17,22,27].

To confirm the role of $NiCo_2S_4$ catalyst in facilitating sulfur reduction reaction (SRR), the rate performances of the three batteries assembled by coupling CNT/S cathode with NCS@SG, CS@SG

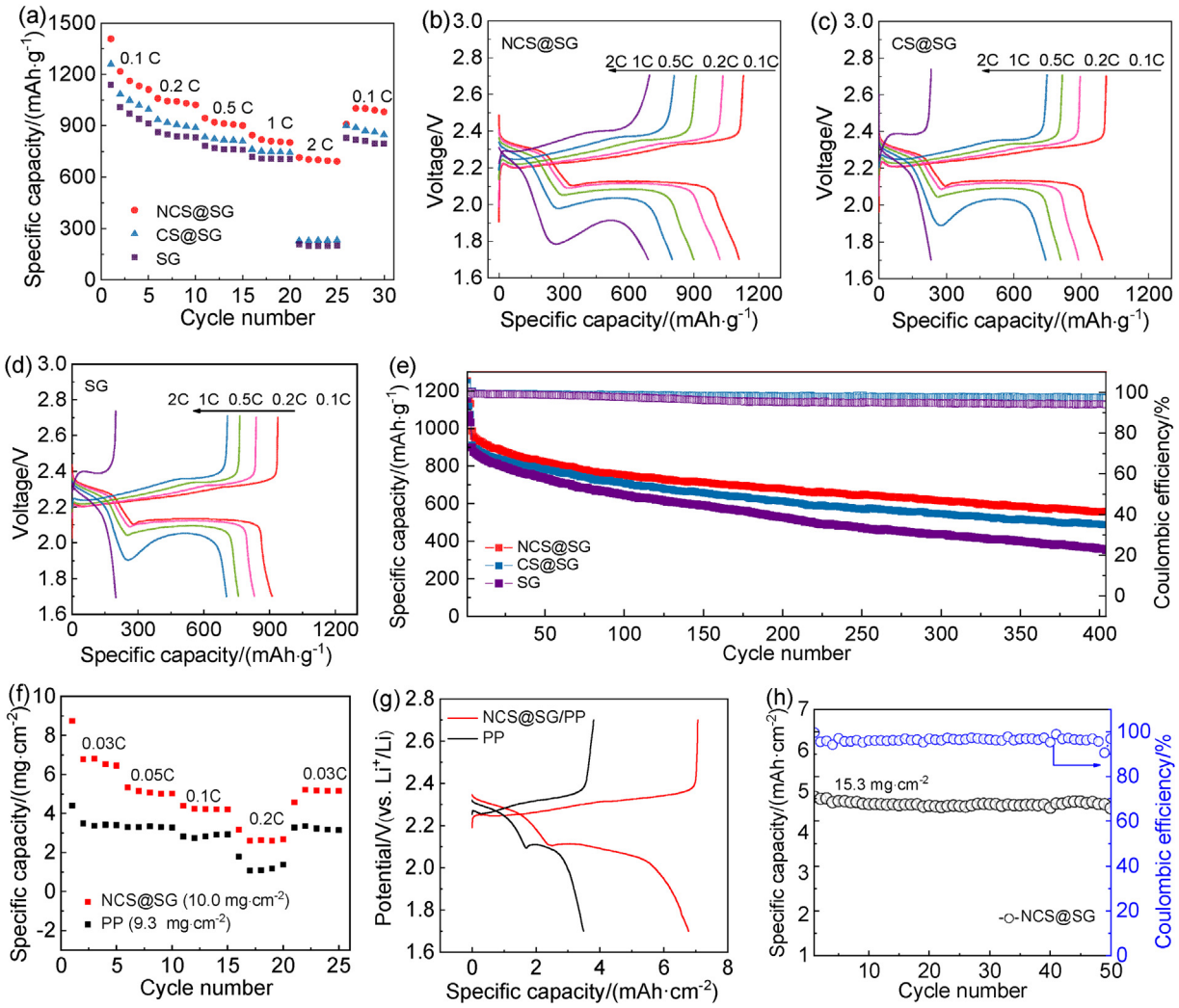

Fig. 5. (a) Rate performance curves of the Li-S batteries with NCS@SG, CS@SG and SG interlayers; (b–d) discharge/charge profiles at different rates; (e) cycling stability at 1.0 C of the three batteries with a sulfur loading of ca. 1.0 mg·cm^{-2}; (f) Rate performance for the freestanding cathodes with or without NCS@SG interlayer and (g) corresponding discharge/charge profiles of the second cycle at 0.03 C; (h) cycling performance of the battery with NCS@SG interlayer with a high sulfur loading at 0.1 C.

and SG interlayers and lithium anode were evaluated (Fig. 5a). An initial capacity of 1408 mAh·g^{-1} at 0.1 C (1.0 C = 1675 mA·g^{-1}) was achieved for the battery with NCS@SG, much higher than those with CS@SG (1260 mAh·g^{-1}) and SG (1140 mAh·g^{-1}). As the current density increases, the capacity difference between NCS@SG and the other two batteries becomes noteworthy. The battery with NCS@SG exhibited much higher capacity at higher rate (713 mAh·g^{-1} at 2.0 C) than those with CS@SG and SG. The galvanostatic charge-discharge curves of the battery with NCS@SG at various current densities (0.1–2.0 C) are shown in Fig. 5b, revealing two distinct discharge plateaus even at 2.0 C. In contrast, the second plateau corresponding to the conversion from LiPSs to Li_2S cannot be observed for the batteries with CS@SG and SG at 2.0 C (Fig. 5c and d). These results clearly confirmed the enhanced SRR process with the $NiCo_2S_4$ catalyst.

The cycling performances of the three batteries are further compared at 1.0 C. As shown in Fig. 5e, the battery with NCS@SG exhibited a high capacity of 559 mAh·g^{-1} after 400 cycles, while the capacities of the batteries with CS@SG and SG quickly decreased to 487 and 354 mAh·g^{-1}, respectively.

To evaluate the potential of NCS@SG interlayer in practical application, freestanding high-sulfur-loading cathodes were prepared (see the preparation details in the Experimental Section) [20]. As shown in Fig. 5f, the battery with NCS@SG interlayer delivered an initial areal capacity of ca. 8.7 mAh·cm^{-2} with a high sulfur areal loading of ca. 10.0 mg·cm^{-2}, much higher than that of the battery without interlayer (4.4 mAh·cm^{-2}). The charge-discharge curves at different rates of the

battery with NCS@SG-modified PP separator or commercial PP separator are shown in Fig. S4a and b. Note that the typical two discharge plateaus of the battery with NCS@SG-modified PP separator are clearly seen at 0.2 C even when the sulfur loading was increased to 10.0 $mg \cdot cm^{-2}$, while the second plateau of the battery with commercial PP separator, corresponding to the conversion of Li_2S_n to Li_2S_2/Li_2S, disappears at such a current. The better rate performance of the battery with NCS@SG-modified PP separator is mainly due to the multiple active centers of the $NiCo_2S_4$ catalyst [46]. In addition, the overpotentials calculated by the voltage difference between the charge and discharge plateaus at different rates are much lower for the battery with NCS@SG-modified PP separator than that with commercial PP separator, confirming the high catalytic activity of $NiCo_2S_4$ catalyst (Fig. 5g and Fig. S4c). [17]. Cycling performance for the free-standing cathodes with NCS@SG interlayer was further evaluated at 0.1 C. As shown in Fig. S5, the NCS@SG battery with 7.4 $mg \cdot cm^{-2}$ sulfur areal loading delivered an initial areal capacity of ca. 3.7 $mAh \cdot cm^{-2}$, and a reversible areal capacity was maintained at 3.2 $mAh \cdot cm^{-2}$ with the retention of 86.5% after 50 cycles. When the areal sulfur loading was increased to 15.3 $mg \cdot cm^{-2}$ (Fig. 5h), an areal capacity of 4.9 $mAh \cdot cm^{-2}$ was obtained, higher than 4.0 $mAh \cdot cm^{-2}$ of commercially available Li-ion batteries [47]. Moreover, the battery could be steadily cycled over 50 cycles with high capacity retention of 93.9%. The remarkable cycling stability with high sulfur loadings confirms the fast conversion of LiPSs with $NiCo_2S_4$ catalyst, which effectively prevents their accumulation from the electrolyte and suppresses the shuttle effect.

4. Conclusions

We demonstrated an effective way of designing a bimetallic sulfide to enhance the catalytic activity of sulfide-based catalysts toward the conversion from LiPSs to Li_2S. The prepared $NiCo_2S_4$ effectively promoted liquid-solid nucleation/deposition of Li_2S, synthetically enhancing the sulfur utilization and suppressing the shuttling of LiPSs. Therefore, the Li-S battery with NCS@SG interlayer showed high-rate capability, stable cycling performance and high Coulombic efficiency. Remarkably, a high areal capacity of 4.9 $mAh \cdot cm^{-2}$ was obtained when the areal sulfur loading increased to 15.3 $mg \cdot cm^{-2}$, and high capacity retention of 93.9% after 50 cycles for such a battery was achieved. This work suggests a proactive strategy to catalyze sulfur redox reactions and provides valuable inspiration for the design of catalysts in Li-S batteries.

Acknowledgements

This work was supported by the National Key R&D Program of China (No. 2021YFF0500600), National Natural Science Foundation of China (Nos. 51932005 and 52022041), All-Solid-State Lithium Battery Electrolyte Engineering Research Centre (XMHT20200203006) and the China Postdoctoral Science Foundation (2022M710041).

References

[1] Bruce P G, Freunberger S A, Hardwick L J, Tarascon J M. Li-O_2 and Li-S batteries with high energy storage[J]. Nat. Mater., 2012, 11: 19−29.
[2] Manthiram A, Chung S H, Zu C X. Lithium-sulfur batteries: progress and prospects[J]. Adv. Mater., 2015, 27(12): 1980−2006.
[3] Chen X, Hou T Z, Persson K A, Zhang Q. Combining theory and experiment in lithium-sulfur batteries: current progress and future perspectives[J]. Mater. Today, 2019, 22: 142−158.
[4] Wang D W, Zeng Q C, Zhou G M, Yin L C, Li F, Cheng H M, Gentle I R, Lu G QM. Carbon-sulfur composites for Li-S batteries: status and prospects[J]. J. Mater. Chem. A, 2013, 1(33): 9382−9394.
[5] Liang X, Hart C, Pang Q, Garsuch A, Weiss T, Nazar L F. A highly efficient polysulfide mediator for lithium-sulfur batteries[J]. Nat. Commun., 2015, 6: 5682.
[6] Ji X L, Lee K T, Nazar L F. A highly ordered nanostructured carbon-sulphur cathode for lithium-sulphur batteries[J]. Nat. Mater., 2009, 8(6): 500−506.
[7] Xin S, Gu L, Zhao N H, Yin Y X, Zhou L J, Guo Y G, Wan L J. Smaller sulfur molecules promise better lithium-sulfur batteries[J]. J. Am. Chem. Soc., 2012, 134(45): 18510−18513.
[8] Zheng G Y, Zhang Q F, Cha J J, Yang Y, Li W Y, Seh Z W, Cui Y. Amphiphilic surface modification of hollow carbon nanofibers for improved cycle life of lithium sulfur batteries[J]. Nano Lett., 2013, 13(3): 1265−1270.
[9] Zhang J T, Hu H, Li Z, Lou X W. Double-shelled nanocages with cobalt hydroxide inner shell and layered double hydroxides outer shell as high-efficiency polysulfide mediator for lithium-sulfur batteries[J]. Angew. Chem. Int. Ed., 2016, 55(12): 3982−3986.
[10] Hua W X, Yang Z, Nie H G, Li Z Y, Yang J Z, Guo Z Q, Ruan C P, Chen X A, Huang S M. Polysulfide-scission reagents for the suppression of the shuttle effect in lithium-sulfur batteries[J]. ACS Nano, 2017, 11(2): 2209−2218.
[11] Fang R P, Zhao S Y, Sun Z H, Wang W, Cheng H M, Li F. More reliable lithium-sulfur batteries: status, solutions and prospects[J]. Adv. Mater., 2017, 29(48): 1606823.
[12] Liu D H, Zhang C, Zhou G M, Lv W, Ling G W, Zhi L J, Yang Q H. Catalytic effects in lithium-sulfur batteries: promoted sulfur transformation and reduced shuttle effect [J]. Adv. Sci., 2018, 5(1): 1700270.
[13] Geng C N, Hua W X, Wang D W, Ling G W, Zhang C, Yang Q H. Demystifying the catalysis in lithium-sulfur batteries: characterization methods and techniques[J]. SusMat, 2021, 1(1): 51−65.
[14] Wang L, Hua W X, Wan X, Feng Z, Hu Z H, Li H, Niu J T, Wang L X, Wang A S, Liu J Y, Lang X Y, Wang G, Li W F,

Yang Q H, Wang W C. Design rules of a sulfur redox electrocatalyst for lithium-sulfur batteries[J]. Adv. Mater., 2022, 34(14): 2110279.

[15] Peng L L, Wei Z Y, Wan C Z, Li J, Chen Z, Zhu D, Baumann D, Liu H T, Allen C S, Xu X, Kirkland A I, Shakir I, Almutairi Z, Tolbert S, Dunn B, Huang Y, Sautet P, Duan X F. A fundamental look at electrocatalytic sulfur reduction reaction[J]. Nat. Catal., 2020, 3(9): 762−770.

[16] Han Z Y, Zhao S Y, Xiao J W, Zhong X W, Sheng J Z, Lv W, Zhang Q F, Zhou G M, Cheng H M. Engineering *d-p* orbital hybridization in single-atom metal-embedded three-dimensional electrodes for Li-S batteries[J]. Adv. Mater., 2021, 33(44): 2105947.

[17] Li Z H, Zhou C, Hua J H, Hong X F, Sun C L, Li H W, Xu X, Mai L Q. Engineering oxygen vacancies in a polysulfide-blocking layer with enhanced catalytic ability[J]. Adv. Mater., 2020, 32(10): 1907444.

[18] Hua W X, Li H, Pei C, Xia J Y, Sun Y F, Zhang C, Lv W, Tao Y, Jiao Y, Zhang B S, Qiao S Z, Wan Y, Yang Q H. Selective catalysis remedies polysulfide shuttling in lithium-sulfur batteries[J]. Adv. Mater., 2021, 33(38): 2101006.

[19] Lin H B, Yang L Q, Jiang X, Li G C, Zhang T R, Yao Q F, Zheng G W, Lee J Y. Electrocatalysis of polysulfide conversion by sulfur-deficient MoS_2 nanoflakes for lithium-sulfur batteries[J]. Energy Environ. Sci., 2017, 10(6): 1476−1486.

[20] Yuan Z, Peng H J, Hou T Z, Huang J Q, Chen C M, Wang D W, Cheng X B, Wei F, Zhang Q. Powering lithium-sulfur battery performance by propelling polysulfide redox at sulfiphilic hosts[J]. Nano Lett., 2016, 16(1): 519−527.

[21] Xia J Y, Hua W X, Wang L, Sun Y F, Geng C N, Zhang C, Wang W C, Wan Y, Yang Q H. Boosting catalytic activity by seeding nanocatalysts onto interlayers to inhibit polysulfide shuttling in Li-S batteries[J]. Adv. Funct. Mater., 2021, 31(26): 2101980.

[22] Sun Z H, Zhang J Q, Yin L C, Hu G J, Fang R P, Cheng H M, Li F. Conductive porous vanadium nitride/graphene composite as chemical anchor of polysulfides for lithium-sulfur batteries[J]. Nat. Commun., 2017, 8: 14627.

[23] Zhou J B, Liu X J, Zhu L Q, Zhou J, Guan Y, Chen L, Niu S W, Cai J Y, Sun D, Zhu Y C, Du J, Wang G M, Qian Y T. Deciphering the modulation essence of p bands in Co-based compounds on Li-S chemistry[J]. Joule, 2018, 2(12): 2681−2693.

[24] Yang Y X, Zhong Y R, Shi Q W, Wang Z H, Sun K N, Wang H L. Electrocatalysis in lithium sulfur batteries under lean electrolyte conditions[J]. Angew. Chem. Int. Ed., 2018, 57(47): 15549−15552.

[25] Zhou T H, Lv W, Li J, Zhou G M, Zhao Y, Fan S X, Liu B L, Li B H, Kang F Y, Yang Q H. Twinborn TiO_2-TiN heterostructures enabling smooth trapping-diffusion-conversion of polysulfides towards ultralong life lithium-sulfur batteries[J]. Energy Environ. Sci., 2017, 10(7): 1694−1703.

[26] Jiao L, Zhang C, Geng C N, Wu S C, Li H, Lv W, Tao Y, Chen Z J, Zhou G M, Li J, Ling G W, Wan Y, Yang Q H. Capture and catalytic conversion of polysulfides by *in situ* built TiO_2-MXene heterostructures for lithium-sulfur batteries[J]. Adv. Energy Mater., 2019, 9(19): 1900219.

[27] Wang R C, Luo C, Wang T S, Zhou G M, Deng Y Q, He Y B, Zhang Q F, Kang F Y, Lv W, Yang Q H. Bidirectional catalysts for liquid-solid redox conversion in lithium-sulfur batteries[J]. Adv. Mater., 2020, 32(32): 2000315.

[28] Zhao M, Peng H J, Zhang Z W, Li B Q, Chen X, Xie J, Chen X, Wei J Y, Zhang Q, Huang J Q. Activating inert metallic compounds for high-rate lithium-sulfur batteries through *in situ* etching of extrinsic metal[J]. Angew. Chem. Int. Ed., 2019, 58(12): 3779−3783.

[29] Zeng P, Liu C, Zhao X F, Yuan C, Chen Y G, Lin H P, Zhang L. Enhanced catalytic conversion of polysulfides using bimetallic Co_7Fe_3 for high-performance lithium-sulfur batteries[J]. ACS Nano, 2020, 14(9): 11558−11569.

[30] Zhou G M, Tian H Z, Jin Y, Tao X Y, Liu B F, Zhang R F, Seh Z W, Zhuo D, Liu Y Y, Sun J, Zhao J, Zu C X, Wu D S, Zhang Q F, Cui Y. Catalytic oxidation of Li_2S on the surface of metal sulfides for Li-S batteries[J]. Proc. Natl. Acad. Sci. U.S.A., 2017, 114(5): 840−845.

[31] Zhang B, Luo C, Deng Y Q, Huang Z J, Zhou G M, Lv W, He Y B, Wan Y, Kang F Y, Yang Q H. Optimized catalytic WS_2-WO_3 heterostructure design for accelerated polysulfide conversion in lithium-sulfur batteries[J]. Adv. Energy Mater., 2020, 10(15): 2000091.

[32] Lv W, Tang D M, He Y B, You C H, Shi Z Q, Chen X C, Chen C M, Hou P X, Liu C, Yang Q H. Low-temperature exfoliated graphenes: vacuum-promoted exfoliation and electrochemical energy storage[J]. ACS Nano, 2009, 3(11): 3730−3736.

[33] Zheng C, Niu S Z, Lv W, Zhou G M, Li J, Fan S X, Deng Y Q, Pan Z Z, Li B H, Kang F Y, Yang Q H. Propelling polysulfides transformation for high-rate and long-life lithium-sulfur batteries[J]. Nano Energy, 2017, 33: 306−312.

[34] Xiao Z B, Yang Z, Wang L, Nie H G, Zhong M E, Lai Q Q, Xu X J, Zhang L J, Huang S M. A lightweight TiO_2/graphene interlayer, applied as a highly effective polysulfide absorbent for fast, long-life lithium-sulfur batteries[J]. Adv. Mater., 2015, 27(18): 2891−2898.

[35] Liu Q, Jin J T, Zhang J Y. $NiCo_2S_4$@graphene as a bifunctional electrocatalyst for oxygen reduction and evolution reactions[J]. ACS Appl. Mater. Interfaces, 2013, 5(11): 5002−5008.

[36] Zhang Z, Shao A H, Xiong D G, Yu J, Koratkar N, Yang Z Y. Efficient polysulfide redox enabled by lattice-distorted Ni_3Fe intermetallic electrocatalyst-modified separator for lithium-sulfur batteries[J]. ACS Appl. Mater. Interfaces, 2020, 12(17): 19572−19580.

[37] Li H, Meng R W, Guo Y, Chen B A, Jiao Y, Ye C, Long Y, Tadich A, Yang Q H, Jaroniec M, Qiao S Z. Reversible electrochemical oxidation of sulfur in ionic liquid for high-voltage Al-S batteries[J]. Nat. Commun., 2021, 12(1): 5714.

[38] Liu B, Huang S Z, Kong D Z, Hu J P, Yang H Y. Bifunctional $NiCo_2S_4$ catalysts supported on a carbon textile interlayer for ultra-stable Li-S battery[J]. J. Mater. Chem., 2019, 7(13): 7604−7613.

[39] Xiao Z B, Yang Z, Li Z L, Li P Y, Wang R H. Synchronous gains of areal and volumetric capacities in lithium-sulfur batteries promised by flower-like porous $Ti_3C_2T_x$ matrix[J]. ACS Nano, 2019, 13(3): 3404−3412.

[40] Al Salem H, Babu G, Rao C V, Arava L MR. Electrocatalytic polysulfide traps for controlling redox shuttle process of Li-S batteries[J]. J. Am. Chem. Soc., 2015, 137(36): 11542−11545.

[41] Hao B Y, Li H, Lv W, Zhang Y B, Niu S Z, Qi Q, Xiao S J, Li J, Kang F Y, Yang Q H. Reviving catalytic activity of nitrides by the doping of the inert surface layer to promote polysulfide conversion in lithium-sulfur batteries[J]. Nano Energy, 2019, 60: 305−311.

[42] Xu K L, Liu X J, Liang J W, Cai J Y, Zhang K L, Lu Y, Wu X, Zhu M G, Liu Y, Zhu Y C, Wang G M, Qian Y T. Manipulating the redox kinetics of Li-S chemistry by tellurium doping for improved Li-S batteries[J]. ACS Energy Lett., 2018, 3(2): 420−427.

[43] Luo L, Chung S H, Manthiram A. Rational design of a dual-function hybrid cathode substrate for lithium-sulfur batteries[J]. Adv. Energy Mater., 2018, 8(24): 1801014.

[44] Shen Z H, Cao M Q, Zhang Z L, Pu J, Zhong C L, Li J C, Ma H X, Li F J, Zhu J, Pan F, Zhang H G. Efficient $Ni_2Co_4P_3$ nanowires catalysts enhance ultrahigh-loading lithium-

sulfur conversion in a microreactor-like battery[J]. Adv. Funct. Mater., 2020, 30(3): 1906661.
[45] Zhao M, Li X Y, Chen X, Li B Q, Kaskel S, Zhang Q, Huang J Q. Promoting the sulfur redox kinetics by mixed organodiselenides in high-energy-density lithium-sulfur batteries[J]. eScience, 2021, 1(1): 44−52.
[46] Zhao M, Peng Y Q, Li B Q, Zhang X Q, Huang J Q. Regulation of carbon distribution to construct high-sulfur-content cathode in lithium-sulfur batteries[J]. J. Energy Chem., 2021, 56: 203−208.
[47] Fang R P, Li G X, Zhao S Y, Yin L C, Du K, Hou P X, Wang S G, Cheng H M, Liu C, Li F. Single-wall carbon nanotube network enabled ultrahigh sulfur-content electrodes for high-performance lithium-sulfur batteries[J]. Nano Energy, 2017, 42: 205−214.

多活性中心双金属硫化物促进多硫化锂转化构建高性能锂硫电池

化五星[a,#]，夏静怡[a,#]，胡忠豪[a]，李　欢[a]，吕　伟[b,*]，杨全红[a,*]
[a] 天津大学化工学院，天津市先进碳与电化学储能重点实验室，天津 300072
[b] 清华大学深圳国际研究生院，深圳市石墨烯重点实验室、炭功能材料工程实验室，广东 深圳 518055

摘要

锂硫电池是极具应用潜力的下一代高能量密度电池体系之一。然而，其充放电中间产物多硫化锂的“穿梭效应”不仅消耗大量电解液，还导致硫活性物质利用率低、循环寿命短，是锂硫电池产业化进程中的主要瓶颈之一。引入催化剂加速硫活性物质转化速率，减少多硫化锂在电解液中的累积浓度，是抑制穿梭效应的有效解决策略。高效的催化剂应具备丰富的催化活性位点，以确保高效吸附多硫化锂并加速其向不溶的充放电产物转化。本文制备出硫掺杂石墨烯表面原位负载的双金属硫化物 $NiCo_2S_4$（NCS@SG）并将其作为催化剂应用于锂硫电池的中间层。相比于单金属硫化物（CoS），$NiCo_2S_4$ 催化剂具有多活性中心催化位点，可以更好地吸附多硫化锂并促进其向放电产物快速转化。应用上述中间层后，电池的充放电比容量、库仑效率和循环稳定性得到了明显提升。当硫的负载达到 15.3 $mg\cdot cm^{-2}$ 时，经过 50 次循环后，具有 NCS@SG 中间层的电池获得了高达 93.9%的容量保持率。上述结果表明，设计双金属基催化剂是优化锂硫电池催化剂活性和反应效率的重要方向。

关键字：锂硫电池；多硫化锂；催化作用；双金属硫化物催化剂；穿梭效应